Author(s): Joo Lee, Young & von Boehm, J. & Nieminen, Risto M.

Title: Simulation of the kinetics of oxygen complexes in crystalline silicon

Year: 2002

Version: Final published version

Please cite the original version:

Joo Lee, Young & von Boehm, J. & Nieminen, Risto M. 2002. Simulation of the kinetics of oxygen complexes in crystalline silicon. Physical Review B. Volume 66, Issue 16. 165221/1-11. ISSN 1550-235X (electronic). DOI: 10.1103/physrevb.66.165221.

Simulation of the kinetics of oxygen complexes in crystalline silicon

Young Joo Lee, J. von Boehm, and R. M. Nieminen
COMP/Laboratory of Physics, Helsinki University of Technology, P.O. Box 1100, FIN-02015 HUT, Finland
(Received 28 March 2002; revised manuscript received 18 June 2002; published 31 October 2002)

The formation kinetics of thermal double donors (TDD's) is studied by a general kinetic model with parameters based on accurate *ab initio* total-energy calculations. The kinetic model includes all relevant association, dissociation, and restructuring processes. The simulated kinetics agrees qualitatively and in most cases quantitatively with the experimentally found consecutive kinetics of TDD's. It also supports our earlier assignments of the ring-type oxygen chains to TDD's [Pesola *et al.*, Phys. Rev. Lett. **84**, 5343 (2000)]. We demonstrate with the kinetic model that the most common assumption that only the O_2 dimer acts as a fast diffusing species would lead to an unrealistic steady increase of the concentration of O_3. The neglect of restructuring processes leads to an anomalous increase of oxygen dimers and negligible concentrations of TDD's. The capture of interstitial oxygens by diffusing oxygen chains and the escaping of interstitial oxygens from the chains fully dominate the formation kinetics.

DOI: 10.1103/PhysRevB.66.165221 PACS number(s): 61.72.Bb, 66.30.−h

I. INTRODUCTION

Thermal donor (TD) families appear in Czochralski-grown Si during annealing.[1–6] It is commonly believed that TD's grow by capturing supersaturated oxygen. The most studied TD family consists of up to 17 thermal double donors (TDD's, TDD0–TDD16) that appear at 350–550 °C.[4,7,8] TDD's grow at an anomalously high formation rate with an activation energy of only 1.7 eV which is about 0.8 eV less than the activation energy of interstitial oxygen atom (O_1) hopping.[9] A popular model used to describe the TDD formation assumes that oxygen dimers (O_2's) act as fast diffusing species (FDS).[5,10,11] In this model there is a common core to which O_2's aggregate to form a series of closely related TDD's. The TDD formation would then proceed as follows:[11–15] $O_2 + \mathrm{TDD}n \rightarrow \mathrm{TDD}(n+1)$. However, the problem with this model is that extremely high values of O_2 diffusivity are required to account for the formation of the initial TDD's.[12] To circumvent this problem, Murin and Markevich[12] suggest that also oxygen trimers (O_3's) should act as FDS. However, Åberg *et al.*[11] conclude that the O_3 formation rate would be three orders of magnitude larger than any other reaction rate of O_2, and reject this possibility in their kinetic model. One could also allow *all* small TDD's to act as FDS as suggested by Murin and Markevich.[12] In this case the TDD formation would proceed as $\mathrm{TDD}n + O_1 \rightarrow \mathrm{TDD}(n+1)$. However, Götz *et al.*[16] argue that the formation and annihilation of TDD's takes place at 550 °C without fast diffusion of oxygen at all. Thus there is a need for a general kinetic model not relying on any specific assumptions to see which of the all possible mechanisms is/are finally responsible for the formation and annihilation of TDD's.

We summarize here briefly the main experimental results that a successful kinetic model should explain. The TDD's appear consecutively.[4,7,8,17] The infrared (IR)-absorption measurements by Åberg *et al.*[11] and the experiments by Claybourn and Newman[18] offer more detailed quantitative data of this kinetics. The total TDD formation rate and the O_1 loss rate show a maximum at 450–500 °C.[2,13,14,19] The corresponding activation energy is 1.2 eV at low temperatures and 1.7–1.8 eV at intermediate temperatures.[18,20,21] The experimental reaction order is 2 at 350–400 °C and increases to 3.5–4 at 450 °C.[19,22,23]

The purpose of this paper is to introduce a general kinetic model and to apply it to the kinetics of oxygen complexes in silicon. The basic ingredients of the model are the activation energies for migration and restructuring as well as the formation and binding energies for various oxygen complexes.[24,25] The model includes the most important processes: diffusion as well as association, dissociation, and restructuring reactions. All possible low-energy structures have to be considered because TDD's are just one of these types.[24,25] The energies of this model are obtained from accurate total-energy calculations, based on the density-functional theory.[24,25] Using the calculated total energies, we have been able to identify oxygen chain structures—consisting of one or more adjacent four-membered rings (*R*) and flanking O_1's—as TDD0–TDD7.[24–26] The *R* unit consists of two threefold coordinated O atoms bonded to two common Si atoms.[27] (Another view would be to consider the inner chain structures to consist of a sequence of alternating *Y*-lid and up-side-down *Y*-lid units.[24–26])

The format of this paper is as follows. A short presentation of diffusion-limited reactions in solids is given in Sec. II. The kinetic model is presented in Sec. III and the parametrization of the model is given in Sec. IV. The results and comparison with experiments are given in Sec. V, and the properties of the kinetic model are considered in Sec. VI. The conclusions are drawn in Sec. VII. Some parts of this work have been published elsewhere[24,28–30] as short reports.

II. DIFFUSION-LIMITED ASSOCIATION AND DISSOCIATION REACTIONS IN SOLIDS

The association reaction between the species *A* and *B* in a solid is limited by the fact that *A* and *B* must first diffuse sufficiently close to each other (typically one or two interatomic distances) to be able to react (see Fig. 1 where this is shown schematically). This state where *A* and *B* are weakly

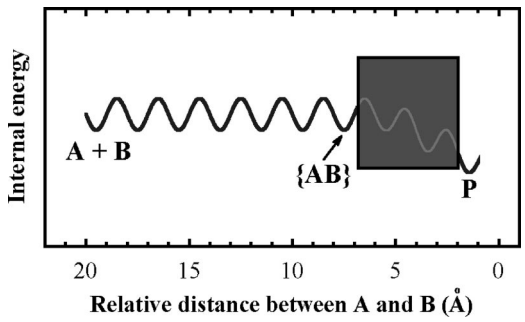

FIG. 1. Schematic diagram of the energy changes as two reactants *A* and *B* are close to each other. The box represents a reaction yielding a product **P**.

bound is denoted by $\{AB\}$. A successful reaction (the box in Fig. 1) yields a product *P*. Competing with this is the dissociation reaction where *P* splits via $\{AB\}$ into the species *A* and *B* (the direction from the right to the left in Fig. 1). The rate equation for the reaction then reads as

$$\frac{d[P]}{dt}=k_a[A][B]-k_d[P], \tag{2.1}$$

where k_a and k_d are the association and dissociation rate constants, respectively. According to Waite's theory,[31] k_a is given as

$$k_a=4\pi R_c(D_A+D_B), \tag{2.2}$$

where R_c is the capture radius and the diffusivities of *A* and *B* are

$$D_A=A_m^A\exp(-E_m^A/k_BT),$$

$$D_B=A_m^B\exp(-E_m^B/k_BT). \tag{2.3}$$

A_m^A and A_m^B are preexponential factors, and E_m^A and E_m^B are activation energies for the migration of species *A* and *B*, respectively. For k_d we use the expression

$$k_d=\frac{A_d}{R_c^2}(D_A+D_B)\exp(-E_b/k_BT), \tag{2.4}$$

where E_b is the binding energy of *P* against the dissociation into *A* and *B*, and A_d is a dimensionless constant.

We note first that k_d is proportional to $\exp(-E_b/k_BT)$ taking into account the splitting of *P* into $\{AB\}$. Second, k_d is proportional to the effective diffusion coefficient D_A+D_B taking into account the diffusion of *A* and *B* in the state $\{AB\}$ towards noninteracting species *A* and *B*. Third, k_d is inversely proportional to R_c^2. In the special case when O_2 splits into two O_1's, k_d is proportional to $\exp[-(E_m+E_b)/k_BT)$ in agreement with the coefficient k_{-2} given in Ref. 12. Also, when one of the species, say *A*, has a much larger diffusivity, k_d is proportional to $\exp[-(E_m^A+E_b)/k_BT)$. In other words, to get rid of *B*, *A* must first overcome the binding energy E_b and then the activation energy for migration E_m^A.

III. KINETIC MODEL FOR REACTIONS OF OXYGEN COMPLEXES IN SILICON

The reactions between oxygen complexes in silicon, including TDD0—TDD16, are much more complex than the simple reaction between *A* and *B* considered in the preceding section. In general, the reactions are of the type

$$O_j+O_k \rightleftharpoons O_{j+k}, \tag{3.1}$$

where O_j denotes a complex containing *j* O atoms and where we neglect the differences between various structures of a certain O_j complex for a moment. The reactions of Eq. (3.1) show the following sequences:

$$O_2+O_1\rightleftharpoons O_3,\ O_3+O_1\rightleftharpoons O_4,\ O_4+O_1\rightleftharpoons O_5, \tag{3.2}$$

$$O_2+O_2\rightleftharpoons O_4,\ O_3+O_2\rightleftharpoons O_5,\ O_4+O_2\rightleftharpoons O_6. \tag{3.3}$$

The reactions in Eqs. (3.2) and (3.3) are *parallel* for O_1 and O_2. On the other hand, the reactions in Eqs. (3.2) and (3.3) are *consecutive* for O_3, O_4, O_5, and so on. Generalizing the kinetic theory [Eqs. (2.1), (2.2), and (2.4) discussed in the preceding section], the rate equations for the reactions of oxygen complexes are given by

$$\frac{d[O_k]}{dt}=\sum_{j=1}^{k-1}(k_a^{j,k-j}[O_j][O_{k-j}]-k_d^{j,k-j}[O_k]) +\sum_{l=1}(1+\delta_{kl})(-k_a^{kl}[O_k][O_l]+k_d^{kl}[O_{k+l}]), \tag{3.4}$$

$$k_a^{kl}=\frac{4\pi R_c}{1+\delta_{kl}}(D_k+D_l), \tag{3.5}$$

$$k_d^{kl}=\frac{A_d^{kl}}{R_c^2}(D_k+D_l)\exp(-E_b^{kl}/k_BT), \tag{3.6}$$

$$D_k=A_m^k\exp(-E_m^k/k_BT), \tag{3.7}$$

where the Kronecker delta δ_{kl} is introduced to avoid double counting.[32] k_a^{kl} is the rate constant for the association reaction of O_k and O_l into O_{k+l}. k_d^{kl} is the rate constant for the dissociation reaction of O_{k+l} into O_k and O_l. D_k denotes the diffusivity and E_m^k the activation energy for the migration of O_k. E_b^{kl} is the binding energy of O_{k+l} against the dissociation into O_k and O_l. In Eq. (3.4), the two terms in the first sum on the right-hand side describe the association of O_j's and O_{k-j}'s into O_k and the dissociation of O_k into O_j's and O_{k-j}'s, respectively. The two terms in the second sum describe the association of O_k's and O_l's into O_{k+l}'s (decreasing $[O_k]$) and the dissociation of O_{k+l}'s into O_k's and O_l's (increasing $[O_k]$), respectively. Equations (3.4)–(3.7) are a generalization to the kinetic models by Murin and Markevich[12] and Götz *et al.*[16]

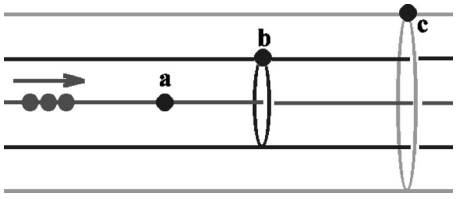

FIG. 2. Schematic view of three different relative distances of interstitial oxygen atoms as seen by an oxygen chain entering along the $[1\bar{1}0]$ axis.

However, the final working equations still need refinements and are considered next. First, the different structures of a complex consisting of a certain number k of O atoms are labeled by an index α: O_k^α. Second, an expression for the restructuring rate V_r—taking into account the restructuring processes within a certain complex—must be added to the right-hand side of Eq. (3.4). V_r is given by

$$V_r = \sum_{\beta \neq \alpha} (k_r^{k\alpha,k\beta}[O_k^\beta] - k_r^{k\beta,k\alpha}[O_k^\alpha]), \tag{3.8}$$

$$k_r^{k\alpha,k\beta} = A_r^{k\alpha,k\beta} \exp(-E_r^{k\alpha,k\beta}/k_B T). \tag{3.9}$$

$k_r^{k\alpha,k\beta}$ is the rate constant for the restructuring reaction from the O_k^β structure into the O_k^α structure, and $E_r^{k\alpha,k\beta}$ is the corresponding activation energy for restructuring. The two terms on the right-hand side of Eq. (3.8) describe the increase of $[O_k^\alpha]$ through restructuring from the other O_k^β structures and the decrease of $[O_k^\alpha]$ through restructuring to the other O_k^β structures, respectively.

IV. PARAMETRIZATION OF THE KINETIC MODEL

The binding energies E_b [Eq. (3.6)], the activation energies for migration E_m [Eq. (3.7)], and the activation energies for restructuring E_r [Eq. (3.9)] have been obtained from accurate total-energy calculations, based on the density-functional theory, and are given in Refs. 28,25. For the determination of the prefactors in Eqs (3.6), (3.7), and (3.9), we specify the labeling of the O complexes as follows. The most important association reactions are due to the processes where an oxygen chain migrating along a $[1\bar{1}0]$ axis captures an O_1, as is shown schematically in Fig. 2. An oxygen chain consisting of $(k-1)$ O atoms may capture an O_1 on the $[1\bar{1}0]$ axis (''*a*'' in Fig. 2), an O_1 in the nearest bond perpendicular to the $[1\bar{1}0]$ axis (''*b*'' in Fig. 2), and an O_1 in a bond more distant but still within the capture radius of ≈ 5 Å (''*c*'' in Fig. 2). The products of these reactions are denoted by O_k^a (an O_k chain), O_k^b (a branched O_k chain), and O_k^c (a branched O_k chain), respectively. The probabilities for the reactions *a*, *b*, and *c* are 1/13, 2/13, and 10/13, respectively,[25] and are included as weighting factors in the association coefficients k_a. The branched O_k^b and O_k^c chains have high activation energies for migration $\geqslant 2.3$ eV.[25] However, the branched O_k^b and O_k^c chains are important in increasing $[O_k^a]$ through restructuring. The calculated activation energies for the restructuring from the branched O_k^b chains to the straight O_k^a chains are 1.9–2.3 eV and those from the branched O_k^c chains to the branched O_k^b chains are 2.3-2.5 eV.[25] The activation energies are thus relatively high. However, the restructuring processes turn out to take less time than the next capture of an O_1 by the migrating straight O_k^a chain.

In our simulations, the oxygen dimer where the two O atoms are bonded to a common Si atom can appear either as the electrically inactive staggered O_2 structure or the electrically active O_{2r} structure[24,25] (O_r denotes an O atom belonging to R). The O_3 chain can appear either as the electrically inactive staggered O_3 structure or the electrically active O_1-O_{2r} structure.[25,26] The O_4 chain can appear either as the electrically inactive staggered O_4 structure, the electrically active asymmetric O_2-O_{2r} structure, or the electrically active symmetric O_1-O_{2r}-O_1 structure.[24–26] The longer O_j chains ($j \geqslant 5$) can appear either as the electrically inactive staggered O_j structure or as the more stable electrically active O_1-O_{nr}-O_1 structure ($n=j-2$).[24–26] We neglect the internal kinetics among various isomer structures within an oxygen dimer or any straight oxygen chain and assume that the thermal equilibrium prevails among the isomer structures. The relative Boltzmann factors $g[\exp(-\Delta E/k_B T)]$ determine the relative abundances of the structures (ΔE is the energy difference between the formation energies of the two structures considered and g takes the degeneracy into account). (In the case of the O_4 chain the relative abundances $[O_2$-$O_{2r}]/[O_1$-O_{2r}-$O_1]$ and $[O_1$-O_{2r}-$O_1]/[$staggered $O_4]$ are used.) This assumption of thermal equilibrium may fail if the energy barrier between the structures is high and/or the temperature is low.

Since it is very difficult to calculate preexponential factors we have resorted to experiments. The preexponential factors are determined as follows. We use for the prefactor A_d/R_c^2 [Eq. (3.6)] the value of 0.4717×10^{15} s^{-1} for the processes where one of the outermost O_1's is moved away from the oxygen chain. This is the value obtained from the reorientation experiments for the well-dispersed oxygen by Stavola *et al.*[33] In all other dissociation and restructuring processes, the common value 0.8772×10^{12} s^{-1} is used for both prefactors A_d/R_c^2 [Eq. (3.6)] and A_r [Eq. (3.9)]. This is the experimental preexponential factor obtained by Stavola *et al.* for the as-provided silicon crystal.[33] For the O_1 diffusivity we use the well-known experimental preexponential factor of $A_m^1 = 0.17$ cm^2 s^{-1} [Eq. (3.7)] by Stavola *et al.*[33] The preexponential factors A_m^{2a}, A_m^{3a}, and A_m^{4a} for the diffusivities of the straight O_2, O_3, and O_4 chains, respectively, are obtained by fitting our calculated $[O_2]$ to the experimental concentration of the 1013-cm^{-1} band (see Refs. 28, 34) at 350 and 420 °C by Åberg *et al.* (Figs. 1(a) and 1(d) in Ref. 11). For the longer chains the diffusivities are geometrically suppressed using the relation $D_k = 0.95 D_{k-1}$ ($k>4$) at $T=450$ °C and electron chemical potential $\mu_e = 0.45$ eV (n-type Si) because there is probably an ''entropic bottleneck,'' which will increasingly hinder the motion of the longer oxygen chains. The corresponding preexponential factors A_m^{ka} are obtained using Eq. (3.7). The relation above is also introduced to keep the number of the fitting parameters small. The calculated

TABLE I. The fitted preexponential factors A_m^{ka} ($cm^2\,s^{-1}$). The electron chemical potential μ_e is 0.45 eV.

k	A_m^{ka}
1	0.17[a]
2	8.58×10^{-10} [b]
3	1.62×10^{-12} [b]
4	1.35×10^{-12} [b]
5	3.42×10^{-11} [c]
6	2.38×10^{-7} [c]
7	2.95×10^{-7} [c]
8	7.44×10^{-6} [c]
9	2.86×10^{-6} [c]
10	1.80×10^{-3} [c]

[a]Experimental value from Refs. 11, 33.
[b]Obtained by fitting the calculated $[O_2]$ to the experimental 1013-cm^{-1} band at 350 and 420 °C (Ref. 11).
[c]Obtained by using the equation $D_k=0.95D_{k-1}$ at 450 °C.

prefactors A_m^{ka} used in our kinetic model are summarized in Table I.

V. RESULTS AND COMPARISON WITH EXPERIMENTS

Figure 3 shows the simulated annealing behavior in *n*-type silicon at 350 °C. All possible structures as well as all association, dissociation and restructuring (including the reorientation of O_2 and O_3) processes are included in the simulation. The simulated annealing behavior of the concentrations of the O_2-O_{2r}, O_1-O_{2r}-O_1, O_1-O_{3r}-O_1, and staggered O_3 chains at 420 °C is given and compared with the IR-absorption experiments[11] in Ref. 28. A more complete simulated annealing behavior displaying also the concentrations of the O_1-O_{2r} and O_1-O_{4r}-O_1 chains as well as of the O_2^b dimer is given in Fig. 4. Figure 4 is also used as the reference to which various simulations performed under different conditions are compared in Sec. VI below. The concentrations of the branched O structures are small ($\leqslant10^{13}$ cm^{-3}) at both 350 and 420 °C and have not been plotted in Figs. 3 and 4. Although the probability of the ''non-head-on'' collisions (leading to branched structures) is significantly larger than that of the ''head-on'' ones, the restructuring reactions toward the (straight) O chains keep the concentrations of the branched structures relatively small. Only in the case of the oxygen dimer the concentration of O_2^b (the skewed O_2) grows so high that it has been plotted. Also in this case the restructuring keeps $[O_2^b]$ lower than the concentration of the staggered O_2 (Figs. 3 and 4). Both the staggered O_2 (the 1060- and 1012-cm^{-1} IR-absorption bands) and O_2^b (the 1105-cm^{-1} IR-absorption band) have been observed simultaneously experimentally[35–37] (for the assignments see Ref. 34). The formation energy of the metastable O_{2r} structure is 0.89 eV higher than that of the staggered O_2, which makes the concentration of O_{2r} negligible (the relative Boltzmann factor $\lesssim3\times10^{-7}$).[25]

At 350 °C the simulated concentration of the O_1-O_{2r} chains (TDD0) is small ($\leqq6\times10^{12}$ cm^{-3}) and is not plotted in Fig. 3. The simulated concentration of the O_1-O_{2r} chains remains still small at 420 °C (Fig. 4). The simulated behavior of the concentration of the staggered O_3 chains at 350 °C agrees closely with that of the experimental 1005-cm^{-1} IR band (Fig. 3) confirming our assignment of the 1005-cm^{-1} band to the staggered O_3 chain in Ref. 28 (see also Fig. 4).

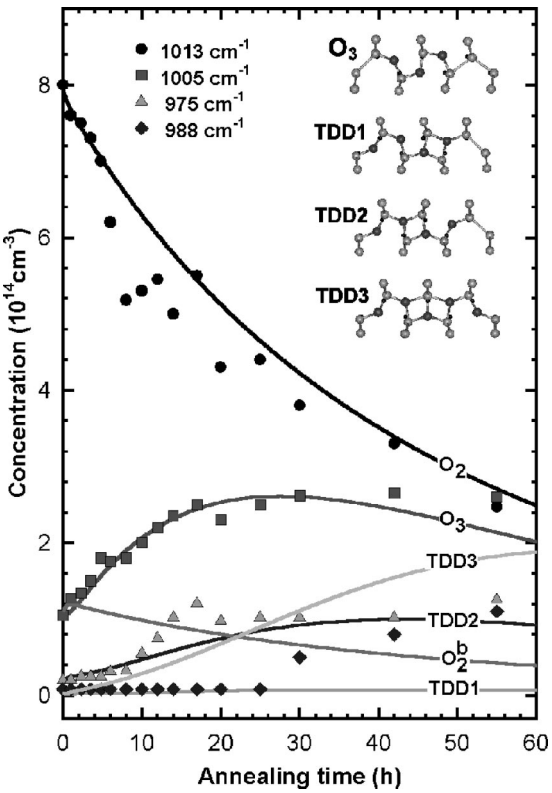

FIG. 3. The simulated annealing at $T=350$ °C for $\mu_e=0.414$ eV and $[O_1]_o=8.28\times10^{17}$ cm^{-3}. The lines represent the simulated results. The calculated band gap equals 0.56 eV. The experimental data points (symbols) obtained from the infrared-absorption experiments by Åberg *et al.* (Ref. 11) are shown for comparison. The theoretical TDD1, TDD2, and TDD3 correspond to the O_2-O_{2r}, O_1-O_{2r}-O_1, and O_1-O_{3r}-O_1 chains, respectively. O_2^b denotes a skewed O dimer, O_2 and O_3 denote staggered O-chains.

We find that at 420 °C the simulated annealing behaviors of the concentrations of the O_2-O_{2r} and O_1-O_{2r}-O_1 chains agree closely with those of the experimental 975- and 988-cm^{-1} IR-absorption bands,[11] respectively, and assign the O_2-O_{2r} and O_1-O_{2r}-O_1 chains to TDD1 (975 cm^{-1}) and TDD2 (988 cm^{-1}), respectively[28] (see also Fig. 4). However, the simulated O_2-O_{2r} concentration at 350 °C in Fig. 3 does not show any initial growth over the O_1-O_{2r}-O_1 concentration in contrast to the experiment by Åberg *et al.*[11] This difference is most probably due to the fact that we neglect the internal kinetics among the O_2-O_{2r}, O_1-O_{2r}-O_1, O_{2r}-O_2, and staggered O_4 structures and weigh these concentrations with the statistical Boltzmann factors. This approach neglects the energy barriers between the structures, which may lead to an erroneous behavior at low temperatures. In *n*-type silicon with $\mu_e=0.414$ eV the O_2-O_{2r} $\rightarrow O_1$-O_{2r}-O_1 and O_{2r}-$O_2\rightarrow O_1$-O_{2r}-O_1 barriers are about 0.4 eV.[25] If the barriers are taken into account, the concentration

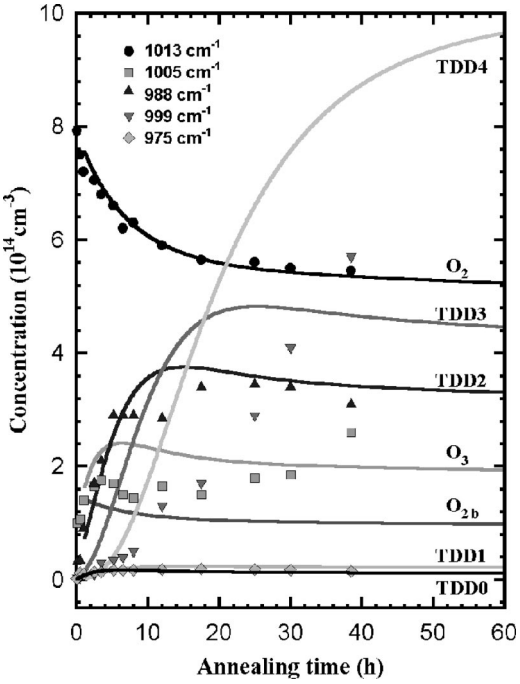

FIG. 4. The simulated annealing at $T=420\,^{\circ}\mathrm{C}$ for $[O_1]_o = 8.28\times10^{17}$ cm^3, and $\mu_e=0.38$ eV. The lines represent the simulated results. The experimental data points (symbols) obtained from the infrared-absorption experiments by Åberg *et al.* (Ref. 11) are shown for comparison. The theoretical TDD0, TDD1, and TDDn ($n>1$) correspond to the O_1-O_{2r}, O_2-O_{2r}, and O_1-O_{nr}-O_1 ($n>1$) chains, respectively. O_2^b denotes a skewed O dimer, O_2 and O_3 denote staggered O chains. The concentrations of the O_2-O_{2r}, O_1-O_{2r}-O_1, O_1-O_{3r}-O_1, and staggered O_3 chains are from Ref. 28.

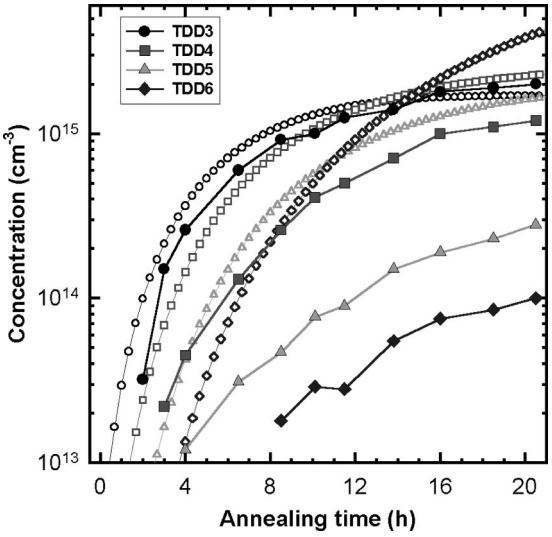

FIG. 5. Simulated concentrations of TDD3-TDD6 (open symbols) as a function of annealing time at 450 °C for $[O_1]_o=1.0\times10^{18}$ cm^{-3} and $\mu_e=0.38$ eV. Theoretical TDDn correspond to the O_1-O_{nr}-O_1 chains, respectively. The experimental data points (filled symbols) are from Ref. 18.

of the O_2-O_{2r} and O_{2r}-O_2 structures (TDD1) increases while that of the O_1-O_{2r}-O_1 structure (TDD2) may decrease. A second possible reason might be the different Fermi energies in the simulation and experiment. The simulated O_1-O_{2r}-O_1 (TDD2) concentration agrees reasonably well with the experimental TDD2 (988 cm^{-1}) concentration in Fig. 3 for longer times ($t>30$ h). And, already at 370 °C and especially at 390 and 420 °C the experimental TDD1 concentration remains below the TDD2 concentration from the beginning of the annealing.[11] The kinetic model gives this behavior. Thus, despite the inconsistency at 350 °C we keep our assignment of the O_2-O_{2r} and O_1-O_{2r}-O_1 chains to TDD1 (975 cm^{-1}) and TDD2 (988 cm^{-1}), respectively.[26]

The experimental 999-cm^{-1} band is assigned to TDD3.[11] We find that at 420 °C the simulated concentration of the O_1-O_{3r}-O_1 chain agrees best with the experimental [TDD3] (see also Fig. 4).[28] However, at 350 °C the O_1-O_{3r}-O_1 concentration starts to grow from the very beginning (Fig. 3), whereas the experimental TDD3 (999 cm^{-1}) concentration (not plotted in Fig. 3) remains negligible. One reason for this difference may again be the fact that we neglect the internal kinetics among the O_1-O_{3r}-O_1 and staggered O_5 structures. The former structure has a formation energy that is about 0.4 eV lower than that of the latter structure.[25] The relative Boltzmann factor makes therefore the O_1-O_{3r}-O_1 structure dominating. The energy barrier from the staggered O_5 structure to the O_1-O_{3r}-O_1 structure is about 0.4 eV.[25] If this barrier is taken into account the concentration of the staggered O_5 structure increases while that of the O_1-O_{3r}-O_1 structure decreases. A second reason could be that the preexponential factor A_m^{5a} (as well as the later factors) in Table I is determined somewhat arbitrarily from the relation $D_k = 0.95 D_{k-1}$ at 450 °C and may give a less satisfactory behavior for TDD5 (and later TDD's). A third reason might be the different Fermi energies in the simulation and experiment. The simulated concentrations of the next O_1-O_{nr}-O_1 chains ($n>3$) show a similar consecutive behavior as the corresponding experimental [TDDn], i.e., the next [TDD(n+1)] grows larger than the previous [TDDn] which has already passed its maximum. Notice that the concentration of the O_1-O_{4r}-O_1 chains (TDD4) grows fast and exceeds that of the O_1-O_{3r}-O_1 chains (TDD3) in Fig. 4 after 20 h. The consecutive reactions at 350 °C in Fig. 3 are seen to take place more slowly than at 420 °C (Fig. 4). This is a natural consequence arising from the fact that the diffusivities of O_1 and O chains [Eq. (3.7)] are significantly lower at 350 °C than at 420 °C.

The agreement found above with the IR-absorption experiments by Åberg *et al.*[11] may be partially due to the fact that the parameters A_m^{2a}, A_m^{3a}, and A_m^{4a} are obtained from fitting to the 1013-cm^{-1} band of the same experiment. Our kinetic model should therefore be compared also with independent experiments. Such a comparison is shown in Fig. 5, where the simulated behaviors of the concentrations of the oxygen chains are compared with the experiments by Claybourn and Newman[18] at 450 °C. However, since different samples may show quite varying behavior the following comparison may only be qualitative or semiquantitative at best. We find that the joint simulated annealing concentration of the O_2-O_{2r} and O_1-O_{2r}-O_1 chains (containing mainly only

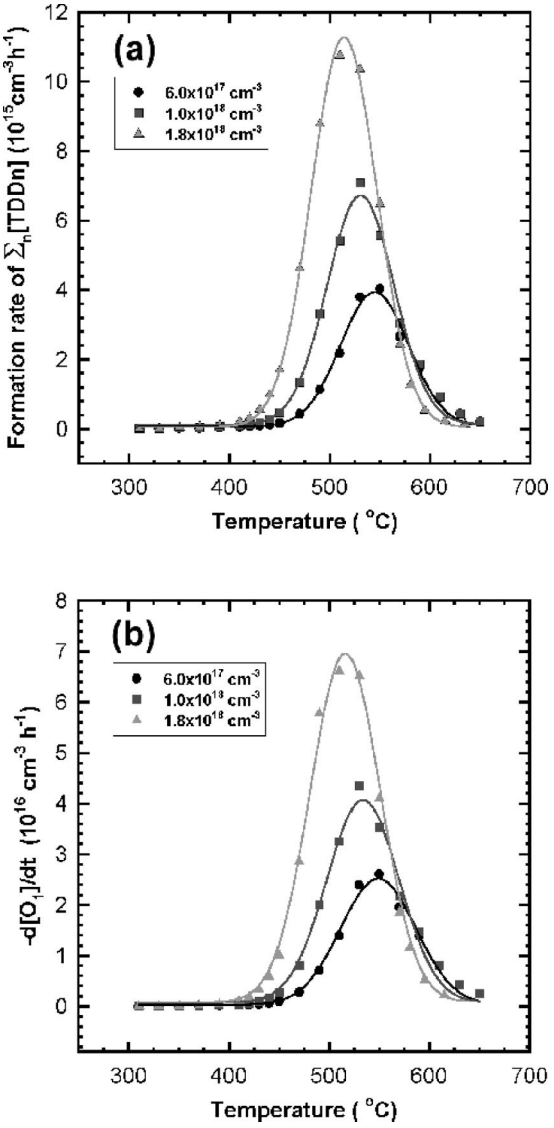

FIG. 6. The calculated TDD formation rates $d\Sigma_n[\mathrm{TDD}n]/dt$ (a) and the calculated interstitial oxygen loss rates (b). $\mu_e = 0.38$ eV. The initial concentrations of interstitial oxygen are given in the inset. The lines are the Gaussian fits to the calculated values. The data for $[\mathrm{O}_1]_o = 1.0 \times 10^{18}$ cm^{-3} is from Ref. 29.

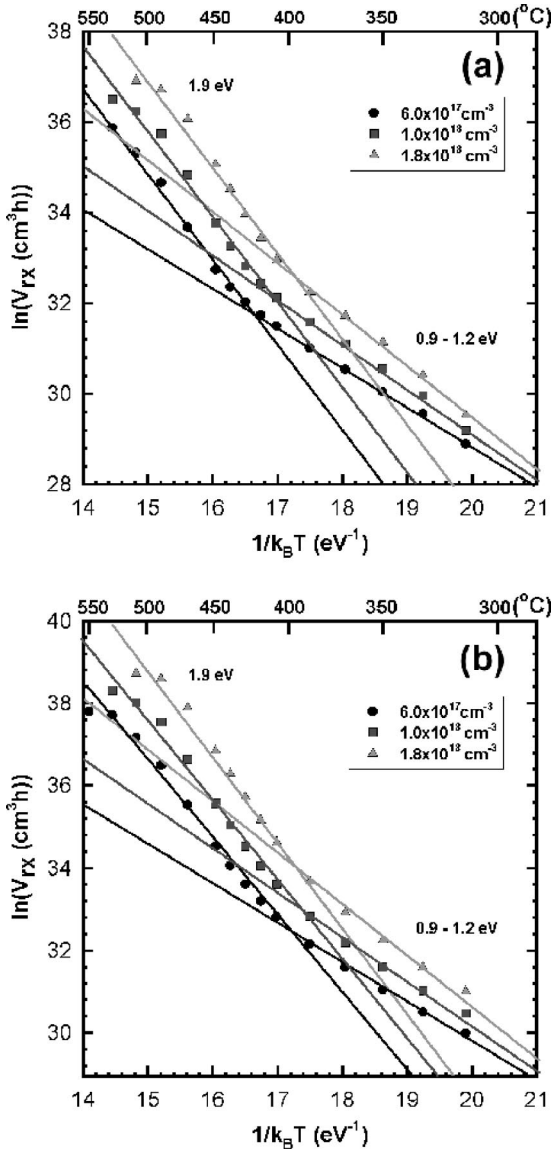

FIG. 7. Arrhenius plots of the calculated formation rates of $d\Sigma_n[\mathrm{TDD}n]/dt$ (a) and the calculated interstitial oxygen loss rates (b). V_{rx} denotes the reaction rate. $\mu_e = 0.38$ eV. The initial concentrations of interstitial oxygen are given in the inset. The lines are linear fits to the calculated values. The data for $[\mathrm{O}_1]_o = 1.0 \times 10^{18}$ cm^{-3} is from Ref. 28.

the latter) - not shown in Fig. 5—lies significantly above the experimental [TDD2], but this difference is not very meaningful because only an unknown proportion of TDD2's was detected in Ref. 18. The simulated behaviors of the concentrations of the O_1-O_{3r}-O_1 and O_1-O_{4r}-O_1 chains in Fig. 5 compare rather closely with the corresponding experimental [TDD3] and [TDD4]. We further find that the simulated concentrations of the O_1-O_{5r}-O_1 and O_1-O_{6r}-O_1 chains behave qualitatively similarly to the corresponding experimental [TDD5] and [TDD6], but the simulated ones grow more steeply than the experimental ones. The reasons for these quantitative differences were considered in the preceding paragraph.

We then consider the overall behavior of simulated TDD's. The calculated early formation rate of TDD's, $d(\Sigma_n[\mathrm{TDD}n])/dt$, and the corresponding loss rate of O_1, $-d[\mathrm{O}_1]/dt$, are shown at different initial O_1 concentrations $[\mathrm{O}_1]_o$ as a function of annealing temperature in Figs. 6(a) and 6(b), respectively. The rates are calculated by using linear fits in the time intervals 0–5 h and 0–2 h for $T \leqslant 550\,^\circ$C and $T > 550\,^\circ$C, respectively. The total TDD formation rates [Fig. 6(a)] and the O_1 loss rates [Fig. 6(b)] are strongly correlated. The O_1 loss rates are about 6.5 times the TDD formation rates. Thus we can conclude that TDD's include about 6.5 O atoms on the average. Both maximum rates increase with increasing $[\mathrm{O}_1]_o$ and shift to lower temperatures as it is natural to expect. The maxima in Fig. 6 are located slightly above 500 °C, which compares reasonably well with the experimental values of 450–500 °C.[2,13,14,19]

Figure 7 shows the calculated total TDD formation rate in

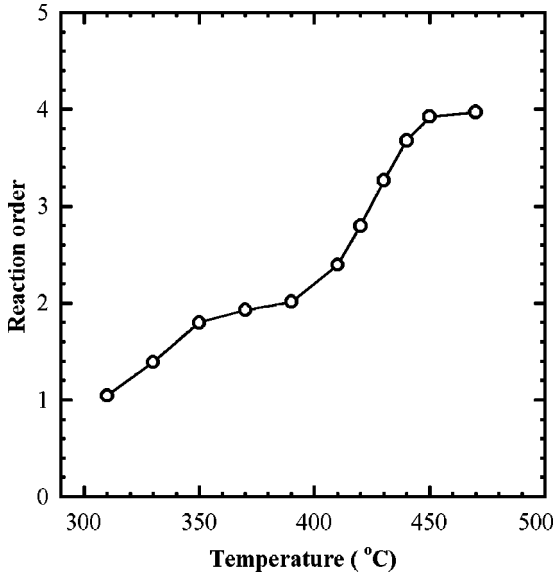

FIG. 8. The calculated reaction order *n*.

logarithmic scale as a function of inverse temperature for various $[O_1]_o$. The kinetic simulations give the activation energies of 0.9–1.2 eV at low temperatures and 1.9 eV at intermediate temperatures.[28,29] The activation energies do not depend sensitively on $[O_1]_o$ at intermediate temperatures, and are in close agreement with the corresponding experimental values of 1.2 and 1.7–1.8.eV.[18,20,21,28,29]

The reaction order *n* in the relation

$$\frac{d\left(\sum_j [\mathrm{TDD}j]\right)}{dt} \sim ([O_1]_o)^n, \tag{5.1}$$

is calculated from the simulations for various $[O_1]_o$ in the same manner as described in Refs. 19, 23. The calculated *n* is shown in Fig. 8. The value of *n* is seen to be 2 at 350–400 °C and to increase to 4 at 450 °C in close agreement with the experimental *n* found to be 2 at 350–400 °C and to increase to 3.5–4 at 450 °C.[19,22,23]

To investigate the annealing time dependences of the TDD concentrations, simulations are carried out for 10 h at 450 °C. The results are show in Fig. 9(a) for $[O_1]_o = 0.6 \times 10^{18}$ cm^{-3} and in Fig. 10(a) for $[O_1]_o = 1.0 \times 10^{18}$ cm^{-3}. The corresponding experimental data points by Emtsev[38] are shown in Figs. 9(b) ($[O_1]_o = 0.65 \times 10^{18}$ cm^{-3}) and 10(b) ($[O_1]_o = 0.8 \times 10^{18}$ cm^{-3}).

The simulated distribution in Fig. 9(a) has the maximum at TDD2 and a growing shoulder at TDD3, indicating a shift from TDD2 to TDD3. Consistently with this Emtsev[38] finds experimentally at later times the maximum at TDD3 [Fig. 9(b)]. Both Figs. 10(a) (simulation) and 10(b) (experiment) show the shift of the maximum from TDD2 to TDD3. Moreover, a growing shoulder at TDD4 is seen in the simulated distribution at 10 h in Fig. 10(a) indicating a further shift of the maximum from TDD3 to TDD4. The experimental relative distribution by Emtsev *et al.*[17] ($T = 450$ °C, $t = 10$ h) displays a distinct maximum at TDD3. Further, the experimental distribution by Götz *et al.*[8] at a slightly higher temperature of $T = 470$ °C and initial concentration of $[O_1]_o = 1.27 \times 10^{18}$ cm^{-3} shows that [TDD4] has grown almost as large as [TDD3] already at $t = 3$ h. Thus, also these experiments indicate a similar consecutive shift of the maximum from TDD3 to TDD4. The kinetic model gives the same shift of the maximum from TDD3 to TDD4 for $t > 10$ h as is obvious from Fig. 4, where [TDD4] grows significantly larger than [TDD3]. The simulated [TDD5] grows later larger than [TDD4] but the stronger growth of [TDD6] seen already as a distinct shoulder in Fig. 10(a) shifts the maximum directly from TDD4 to TDD6. This is due to the fact that the corresponding O_1-O_{6r}-O_1 chain has a lower formation energy (Fig. 3 in Ref. 26) than the previous O_1-O_{5r}-O_1 chain and has a relatively high binding energy against the dissociation ($O_8 \rightarrow O_7 + O_1$) (see Fig. 16 in Ref. 25).

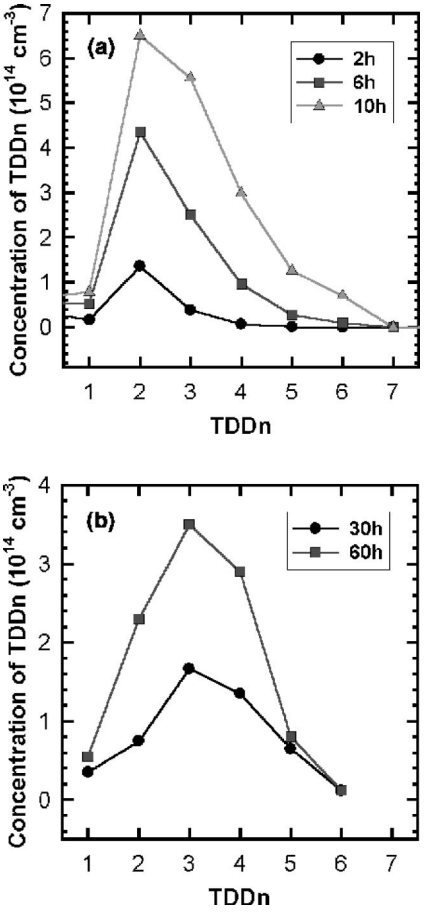

FIG. 9. (a) Simulated concentrations of thermal double donors as a function of annealing time at 450 °C for $[O_1]_o = 0.6 \times 10^{18}$ cm^{-3}. $\mu_e = 0.38$ eV. TDD0, TDD1, and TDD*n* ($n > 1$) correspond to the O_1-O_{2r}, O_2-O_{2r} and O_1-O_{nr}-O_1 ($n > 1$) chains, respectively. (b) The experimental concentrations by Emtsev (Ref. 38) at 450 °C for $[O_1]_o = 0.65 \times 10^{18}$ cm^{-3}.

Figure 11 shows the effect of temperature on the simulated [TDD*n*] distribution at 4 h. The main effect of increasing temperature is to increase all concentrations of TDD's. This is a direct consequence of the fact that the rate constants in Eqs. (3.4) and (3.8) increase proportional to a Boltzmann factor with increasing temperature. The relatively rapid

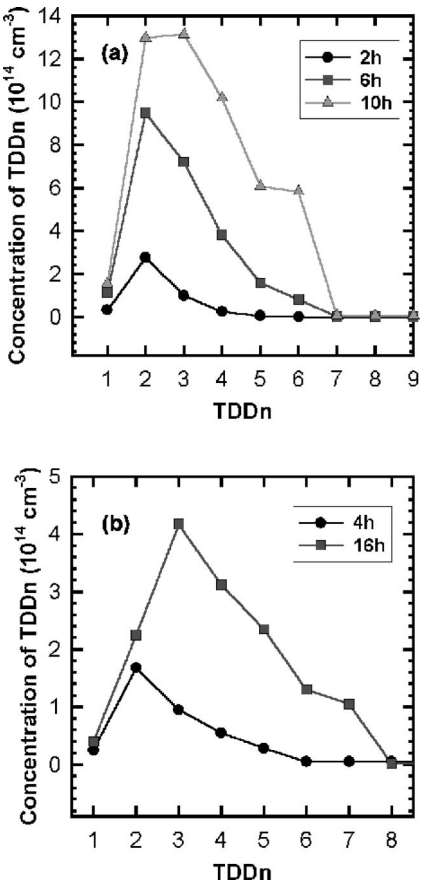

FIG. 10. (a) Simulated concentrations of thermal double donors as a function of annealing time at 450 °C for $[O_1]_o = 1.0 \times 10^{18}$ cm^{-3}. $\mu_e = 0.38$ eV. TDD0, TDD1, and TDDn ($n>1$) correspond to the O_1-O_{2r}, O_2-O_{2r}, and O_1-O_{nr}-O_1 ($n>1$) chains, respectively. (b) The experimental concentrations by Emtsev (Ref. 38) at 450 °C for $[O_1]_o = 0.8 \times 10^{18}$ cm^{-3}.

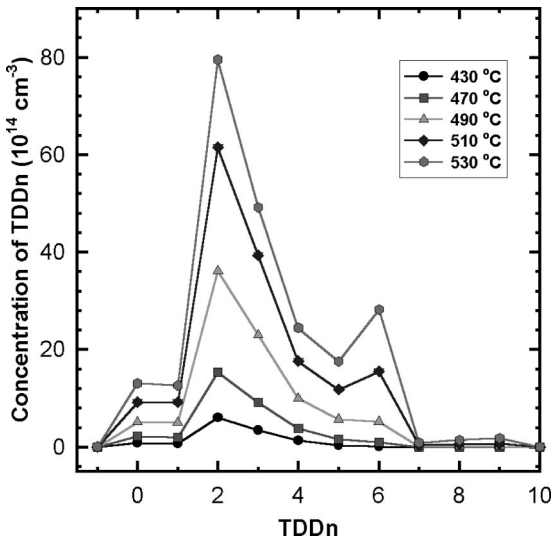

FIG. 11. Simulated concentration of thermal double donors at different temperatures at 4 h annealing. The initial concentration of O_1 is 1.0×10^{18} cm^{-3} and the electron chemical potential $\mu_e = 0.38$ eV. TDD0, TDD1, and TDDn ($n>1$) correspond to the O_1-O_{2r}, O_2-O_{2r}, and O_1-O_{nr}-O_1 ($n>1$) chains, respectively.

growth of the TDD6 concentration is due to the fact that the corresponding O_1-O_{6r}-O_1 chain has a lower formation energy than the previous O_1-O_{5r}-O_1 chain.

VI. PROPERTIES OF THE KINETIC MODEL

Since the simulated results above agree quite closely with experiments and since the kinetic model is fairly general including all association, dissociation, and restructuring processes, we are able to investigate the effects caused by the assumptions used in the other models. The simulated annealing at $T = 420$ °C of Fig. 4 is used here as the representative reference.

First, we study the case where only the O_2 dimer acts as a fast diffusing species. This is achieved simply by setting all diffusivities except for D_2 equal to D_1 (from Table I $D_2 = 1850 D_1$ at $T = 420$ °C, and D_2 is thus much larger than D_1). The result is shown in Fig. 12. The most striking feature in Fig. 12 is the anomalous steady increase of the concentration of the staggered O_3 chains—a feature not present in our kinetic simulation in Fig. 4. Due to the anomalous growth of the concentration of the O_3 trimers, Åberg *et al.*[11] rejected this possibility from their kinetic model. This increase is due to the fact that the O_3 chains can capture almost no O_1's due to their very low diffusivity ($D_3 = D_1$). Thus, practically no O_4 or longer chains can be formed. This should be contrasted to the behavior in Fig. 4 where the several TDD's have developed consecutively within the same time. Thus, the simultaneous inclusion of fast diffusion of *all* O chains is essential. It has been noticed earlier[10,11] that the use of only O_2 as a fast diffusing species in a kinetic model would require unreasonably high diffusivities of $\sim 10^6 D_1 - 10^8 D_1$ for O_2 if the behavior matches the effective oxygen diffusivities of $\sim 10^4 D_1$ determined from precipitation[39,40] and out-diffusion[41,42] experiments.

We consider next a situation where both O_2 and O_3 act as fast diffusing species.[12] At 420 °C all dissociation processes (such as $O_4 \rightarrow O_3 + O_1$ and $O_4 \rightarrow O_2 + O_2$) can be neglected at least up to 60 h as will be discussed later in this paper. A simulation at 420 °C is expected to lead to the following behavior. Owing to its high mobility O_3 can now capture O_1's and $[O_3]$ is not expected to grow anomalously any more. However, the concentrations of the staggered O_4, O_2-O_{2r} (TDD1), and O_1-O_{2r}-O_1 (TDD2) chains are now expected to grow anomalously like $[O_3]$ in Fig. 12 because these O_4 chains are not able to capture O_1's due to their low diffusivities ($D_4 = D_1$). But this kind of anomalous growth of $[O_4]$, [TDD1] or [TDD2] has not been observed experimentally.

To see the effect of restructuring from branched O chains to straight O chains, we have performed a simulation neglecting all restructuring [i.e., the restructuring constants k_r in Eq. (3.8) are set equal to zero]. The result of the simulation is shown in Fig. 13. The concentrations of the weakly bound O_2^c and O_2^b dimers (O_2^b is the skewed O_1-Si-Si-O_1 structure[26]) are seen to increase anomalously due to the O_1-O_1 collisions. There are two reasons for this increase. First, the O_2^c and O_2^b dimers have high activation energies for

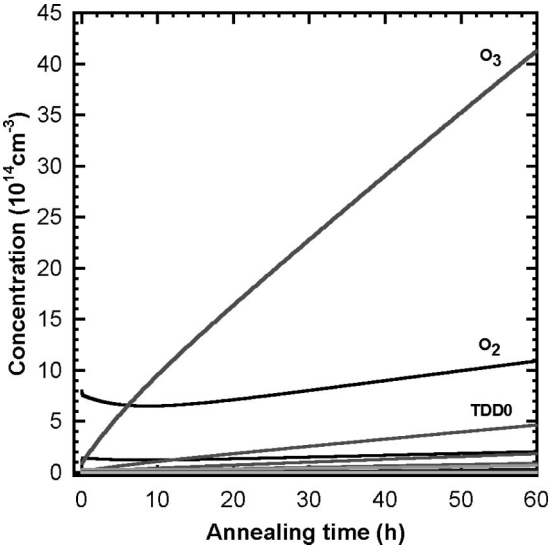

FIG. 12. The simulated annealing at $T=420\,^{\circ}\mathrm{C}$ for $[O_1]_o = 8.28\times10^{17}$ cm^3 and $\mu_e=0.38$ eV with the assumption that all diffusivities except for D_2 equal D_1. TDD0 denotes the O_1-O_{2r} chain. The bunch of lines below 2×10^{14} cm^3 includes the O_2-O_{2r} (TDD1) and O_1-O_{nr}-O_1 (TDDn) ($n>1$) chains, the staggered O chains, as well as the branched structures.

migration and are not able to capture O_1's to form O_3 complexes. Second and more important, O_2^b and O_2^c (via O_2^b) are not allowed to restructure into the staggered O_2 dimer. Therefore, there are no mechanisms that would decrease $[O_2^c]$ and $[O_2^b]$. At the same time the concentration of staggered O_2 cannot increase via restructuring, and therefore $[O_2]$ remains significantly lower than $[O_2^c]$ and $[O_2^b]$ in Fig. 13, whereas in the full simulation including restructuring $[O_2]$ is significantly larger than $[O_2^b]$ and $[O_2^c]$ (Fig. 4). The staggered O_2 dimers may capture O_1's to form mainly branched O_3^c and O_3^b trimers and to less extent straight O_3

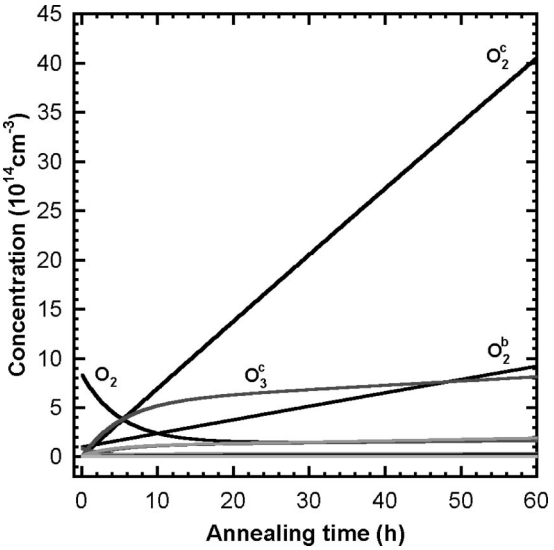

FIG. 13. The simulated annealing at $T=420\,^{\circ}\mathrm{C}$ for $[O_1]_o = 8.28\times10^{17}$ cm^3 and $\mu_e=0.38$ eV when all restructuring is neglected.

TABLE II. Summary of the main simulated results.

Property	Simulation	Experiment
TDD's appear consecutively?	YES	YES[a]
TDD-rate and O_1-loss-rate maximum	500 °C	450–500 °C[b]
Low-T activation energy	0.9–1.2 eV	1.2 eV[c]
Intermediate-T activation energy	1.9 eV	1.7–1.8 eV[c]
Reaction order n	$2\rightarrow4$	$2\rightarrow3.5\cdots4$[d]

[a]References 4, 7, 8, 17, 38.
[b]References 2, 13, 14, 19.
[c]References 18, 20, 21.
[d]References 19, 23, 22.

trimers. The branched O_3^c and O_3^b trimers have high activation energies for migration and cannot restructure into straight O_3 trimers. Since only a small amount of straight O_3 trimers may further capture O_1's on their axis, the total concentration of the O_k chains for $k\geqslant4$ (including the later TDD's) remains less than 2×10^{14} cm^{-3}. Again, this behavior should be contrasted with the full simulation in Fig. 4 where restructuring is included, and where several TDD's have developed consecutively within the same time. Thus, the head-on collisions alone are not sufficient to develop the TDD series, but restructuring from branched structures into chains (included in Fig. 4) is crucial.

Dissociation is often neglected in kinetic models. We have studied the effects due to the neglect of dissociation by simply setting the dissociation coefficients k_d in Eq. (3.4) equal to zero. We find that the dissociation reactions are not important at low temperatures 350–420 °C where the formation of TDD's plays the main role. However, at higher temperatures the dissociation is of main importance in causing the disappearance of TDD's.

We studied the contribution of all association and dissociation reactions where O_1 is not involved, i.e., the reactions

$$O_j + O_k \rightleftharpoons O_{j+k}, \quad j,k>1 \tag{6.1}$$

by neglecting these reactions in the simulation. The result of the simulation at 420 °C including only the captures and escapes of O_1 (as well as restructuring) gives virtually the same result that is obtained with the full simulation (Fig. 4). This shows that the captures and escapes of O_1's fully dominate the consecutive reactions of the TDD formation.

VII. SUMMARY AND CONCLUSIONS

The formation kinetics of thermal double donors is studied by a general kinetic model, which is based on accurate *ab initio* total-energy calculations. The kinetic model includes all relevant association, dissociation, and restructuring processes. We give a brief summary of the main simulated results compared with experiments in Table II.

The simulated kinetics agrees qualitatively and in most cases quantitatively with the experimentally found consecu-

tive kinetics of thermal double donors, supporting at the same time our earlier assignments of the ring-type oxygen chains to thermal double donors. Due to the generality of the kinetic model, we were able to study some of the most common assumptions used in other kinetic models. We demonstrate that the popular assumption that only the O_2 dimer acts as a fast diffusing species leads to an unrealistic steady increase of $[O_3]$. The neglect of the restructuring of branched oxygen chains leads to an anomalous increase of the weakly bound O_2^c dimers and the skewed O_1-Si-Si-O_1 (O_2^b) dimers, and to negligible concentrations of other oxygen chains (and thus TDD's). The neglect of dissociation works at low temperatures (350–420 °C) where the formation processes are dominating, but at higher temperatures the dissociation processes become increasingly important. Finally, we demonstrate that the captures of interstitial oxygens by oxygen chains and the escapes of interstitial oxygens from oxygen chains (as well as restructuring) fully dominate the formation kinetics of the thermal double donors.

ACKNOWLEDGMENT

This work has been funded by Academy of Finland through the Center of Excellence Program (2000-2005). The authors would like to thank Dr. M. Pesola, Professor M. J. Puska, and Professor V. V. Emtsev for valuable discussions. In addition, the authors would like to thank Professor V. V. Emtsev for giving us unpublished experimental data as well as for the permission to refer to it. We acknowledge the generous computing resources of the Center for the Scientific Computing (CSC), Espoo, Finland. Y. J. Lee would like to thank Mr. O. Jääskeläinen for his generous support in computation.

[1] C. S. Fuller, J. A. Ditzenberger, N. B. Hannay, and E. Buehler, Phys. Rev. **96**, 833 (1954).
[2] V. Cazcarra and P. Zunino, J. Appl. Phys. **51**, 4206 (1980).
[3] H. Navarro, J. Griffin, J. Weber, and L. Genzel, Solid State Commun. **58**, 151 (1986).
[4] P. Wagner and J. Hage, Appl. Phys. A: Solids Surf. **A49**, 123 (1989).
[5] *Early Stages of Oxygen Precipitation in Silicon*, edited by R. Jones (Kluwer Academic, Dordrecht, The Netherlands, 1996).
[6] C. A. J. Ammerlaan, in *Properties of Crystalline Silicon*, edited by R. Hull (INSPEC, London, 1999), p. 663.
[7] B. Pajot, H. Compain, J. Lerouille, and B. Clerjand, Physica B & C **117B&118B**, 110 (1983).
[8] W. Götz, G. Pensl, and W. Zulehner, Phys. Rev. B **46**, 4312 (1992).
[9] J. C. Mikkelsen, in *Oxygen, Carbon, Hydrogen, and Nitrogen in Crystalline Silicon*, edited by J. C. Mikkelson, Jr., S. J. Pearton, J. W. Corbett, and S. J. Pennycook, Mater. Res. Soc. Symp. Proc. No. **59** (Materials Research Society, Pittsburgh, 1986), p. 19.
[10] U. Gösele and T. Y. Tan, Appl. Phys. A: Solids Surf. **A28**, 79 (1982).
[11] D. Åberg, B. G. Svensson, T. Hallberg, and J. L. Lindström, Phys. Rev. B **58**, 12 944 (1998).
[12] L. I. Murin and V. P. Markevich, in *Early Stages of Oxygen Precipitation in Silicon*, edited by R. Jones (Kluwer Academic, Dordrecht, The Netherlands, 1996) p. 329.
[13] R. C. Newman, in *Early Stages of Oxygen Precipitation in Silicon*, edited by R. Jones (Kluwer Academic, Dordrecht, The Netherlands, 1996) p. 19.
[14] R. C. Newman, Mater. Sci. Eng., B **36**, 1 (1996).
[15] M. P. Guse and R. Kleinhenz, J. Appl. Phys. **72**, 4615 (1992).
[16] W. Götz, G. Pensl, W. Zulehner, R. C. Newman, and S. A. McQuaid, J. Appl. Phys. **84**, 3561 (1998).
[17] V. V. Emtsev, B. A. Andreev, A. Misiuk, W. Jung, and K. Schmalz, Appl. Phys. Lett. **71**, 264 (1997).
[18] M. Claybourn and R. C. Newman, Appl. Phys. Lett. **51**, 2197 (1987).
[19] S. A. McQuaid, M. J. Binns, C. A. Londos, J. H. Tucker, A. R. Brown, and R. C. Newman, J. Appl. Phys. **77**, 1427 (1995).
[20] V. P. Markevich, L. F. Makarenko, and L. I. Murin, Phys. Status Solidi A **97**, K1 73 (1986).
[21] T. Hallberg and J. L. Lindström, Mater. Sci. Eng., B **B36**, 13 (1996).
[22] W. Kaiser, H. L. Frisch, and H. Reiss, Phys. Rev. **112**, 1546 (1958).
[23] C. A. Londos, M. J. Binns, A. R. Brown, S. A. McQuaid, and R. C. Newman, Appl. Phys. Lett. **62**, 1525 (1993).
[24] Y. J. Lee and R. M. Nieminen, Comput. Phys. Commun. **142**, 305 (2001).
[25] Y. J. Lee, J. von Boehm, M. Pesola, and R. M. Nieminen, Phys. Rev. B **65**, 085205 (2002).
[26] M. Pesola, Y. J. Lee, J. von Boehm, M. Kaukonen, and R. M. Nieminen, Phys. Rev. Lett. **84**, 5343 (2000).
[27] L. C. Snyder, J. W. Corbett, P. Deák, and R. Wu, in *Defects in Electronic Materials*, edited by M. Stavola, S. J. Pearton, and G. Davies, Mater. Res. Soc. Symp. Proc. No. **104** (Materials Research Society, Pittsburgh, 1988), p. 179.
[28] Y. J. Lee, J. von Boehm, M. Pesola, and R. M. Nieminen, Phys. Rev. Lett. **86**, 3060 (2001).
[29] Y. J. Lee, J. von Boehm, and R. M. Nieminen, Appl. Phys. Lett. **79**, 1453 (2001). Note that in the caption of Fig. 3 ''1.0'' should be replaced by ''1.8.''
[30] Y. J. Lee and R. M. Nieminen, *Defect and Diffusion Forum* (Scitec Publications, Switzerland, 2001), Vols. 194–199, p. 261.
[31] T. R. Waite, Phys. Rev. **107**, 463 (1957).
[32] R. A. Alberty, *Physical Chemistry* (Wiley, New York, 1983).
[33] M. Stavola, J. R. Patel, L. C. Kimerling, and P. E. Freeland, Appl. Phys. Lett. **42**, 73 (1983).
[34] M. Pesola, J. von Boehm, and R. M. Nieminen, Phys. Rev. Lett. **82**, 4022 (1999).
[35] T. Hallberg, J. L. Lindström, L. I. Murin, and V. P. Markevich, Mater. Sci. Forum **258-263**, 361 (1997).
[36] L. I. Murin, T. Hallberg, V. P. Markevich, and J. L. Lindström, Phys. Rev. Lett. **80**, 93 (1998).

[37] S. Öberg, C. P. Ewels, R. Jones, T. Hallberg, J. L. Lindström, L. I. Murin, and P. R. Briddon, Phys. Rev. Lett. **81**, 2930 (1998).
[38] V. V. Emtsev (private communication).
[39] H. Takeno, Y. Hayamizu, and K. Miki, J. Appl. Phys. **84**, 3113 (1998).
[40] W. Bergholz, J. L. Lutchison, and P. Pirouz, J. Appl. Phys. **58**, 3419 (1985).
[41] S. A. McQuaid, B. K. Johnson, D. Gambaro, R. Falster, M. J. Ashwin, and J. H. Tucker, J. Appl. Phys. **86**, 1878 (1999).
[42] S.-T. Lee and P. Fellinger, Appl. Phys. Lett. **49**, 1793 (1986).